OBSERVING THE VARIABILITY OF AGN: APERTURE PHOTOMETRY VS. PSF FITTING

by

Eric C. Allan

A senior thesis submitted to the faculty of

Brigham Young University

in partial fulfillment of the requirements for the degree of

Bachelor of Science

Department of Physics and Astronomy

Brigham Young University

August 2007

BRIGHAM YOUNG UNIVERSITY

DEPARTMENT APPROVAL

of a senior thesis submitted by

Eric C. Allan

This thesis has been reviewed by the research advisor, research coordinator, and department chair and has been found to be satisfactory.

Date	J. Ward Moody, Advisor
Date	Eric Hintz, Research Coordinator
Date	Ross Spencer, Chair

ABSTRACT

OBSERVING THE VARIABILITY OF AGN: APERTURE PHOTOMETRY VS. PSF FITTING

Eric C. Allan

Department of Physics and Astronomy

Bachelor of Science

Photometry of galactic nuclei is a difficult task due mainly to extreme obscuration and light contamination from the nuclear bulge. To reach accuracy levels that are of interest astrophysically (on the order of 0.05 to 0.001 magnitudes) requires careful observing techniques and special reduction algorithms. In this paper we make a comparison between standard aperture photometry and DAO photometry–a point spread fitting technique–to illustrate the pros and cons of using these techniques to obtain brightnesses of galactic nuclei. We will show that the DAO method seems to be more effective in all cases, but its accuracy is inconclusive. We will provide some data for a further comparison between these two techniques and a third bulge fitting technique.

ACKNOWLEDGMENTS

I would like to thank my research partner Adam Johanson for helping me along the way. I would also like to thank my research mentor Dr. Moody for helping me learn what it's like to be a scientist. I would also like to thank the guys at tech support for always keeping the Linux machines up to snuff.

I would like to thank Tenagra Observatories for sending us these images. We couldn't have done it without them.

I would also like to thank my wife who supported me as I worked on this project.

Contents

List of Figures

Chapter 1

Introduction

Active Galactic Nuclei (AGN) are characterized by several factors including a bright un-resolved source, highly variable brightness and emission by non-thermal radiation which is usually Inverse Compton Scattering or synchrotron radiation. They are extremely luminous. The variability range can cover several magnitudes while the varability rate is as short as a few days or even several hours. Light travel time arguments on the variability constrain the varying region to be on the order of the size of the solar system.

The small size of AGN coupled with their rapid variability constrain the possible causes of this heavily studied phenomenon. The standard model for AGN assumes that their luminosity stems from supermassive black holes (of order 106 - 109 times solar) at the centers of the galaxies. [Carrol et al. (1996)] The black holes form accretion disks as gravity-captured matter spirals into them. The matter undergoes a huge loss of potential energy as it approaches the black hole. This energy loss is converted to electromagnetic radiation, which interacts with the halo of gas and dust surrounding the black hole.

Recent studies also indicate that black holes are probably present at the center

of every galaxy. [Van der Marel (1999)] This evidence comes from observing velocity dispersion profiles of the galaxian bulges. That is, nearly all galaxies show an increase in stellar velocities in their centers that is consistent with the presence of a supermassive black hole. If this is true, then we should be able to observe the same characteristics of AGN in every normal galaxy as well, though perhaps on a relatively small level.

1.1 Significance

The amount of variability in a normal galactic nucleus is hard to predict. But it is safe to assume that it would be smaller in magnitude range than a typical AGN. Therefore in order to observe these fluctuations in a normal galaxy, we need to determine the most accurate method of photometry for extended objects like galaxies. Most of the methods currently used were developed for point sources like stars. Galaxy nuclei may often be stellar-like sources but they are surrounded by resolved bulges containing hundreds of millions of stars. The bulge light creates problems with both aperture photometry and with point-spread function (PSF) fitting techniques such as DAOphot. My research partner's previous results were inconclusive as to which of these two methods was more accurate. [Johanson (2007)] We will attempt to clarify this ambiguity.

A new method, proposed by professor Stephen McNeil from BYU Idaho as part of his thesis work [McNeil (2004)], uses bulge light as a reference against which nuclear light can be compared. The light coming from the bulge originates from billions of stars, and should be stable down to millimagnitudes. This bulge referencing method carefully maps the bulge light using concentric apertures then subtracts them from their neighbors to find the amount of light in each ring.

We intend to perform the best aperture photometry on galaxy nuclei that could possibly be done. We will do these preliminary measurements to provide data for a comparison with Professor McNeil's method. This will hopefully give credibility to the new bulge fitting technique and pave the way for an extensive observation of galactic nuclei. In the end, this study will provide insights into the obscuring bulges of galactic nuclei and allow us to probe around the black holes. If this method can be perfected it will give additional evidence for the existence of black holes in every galaxy and will possibly allow us to understand a little more about galactic evolution.

Chapter 2

Observations

2.1 Tenagra

Figure 2.1 Tenagra II telescope. Source:www.tenagraobservatories.com

All images used in this project were obtained from the Tenagra Observatory 32 telescope. The observatory is situated in the Sonora desert in southern Arizona. The 32 telescope is an automated observatory that opens at dusk and closes at dawn automatically. It is programmed to take a series of calibration frames and then begin

tracking its assigned targets. The station is also equipped to monitor the weather—clouds, humidity, temperature, etc.—and will close down automatically in case of wind, rain, dew, or other potentially harmful conditions. The arid climate of Arizona provides good seeing conditions with extremely low humidity. [Schwartz (2007)]

The CCD used to take our frames was a SITe 1024 x 1024. Frames were taken in the Johnson B, V, and R filters nearly every night. The plate scale is about 0.87 arcsec per pixel, with a 14.8 arcmin x 14.8 arcmin field of view. The limiting magnitude is 22 with a five minute unfiltered exposure.

Below is a table of the objects that we observed with the date of the observation and the filter used. Column one gives the date of observation in universal time. Columns two, three and four give the filters used on M81, M101, and M51 respectively. A blank entry in these latter columns means we have no data for that object on that particular night. B,V, or R represents frames taken in Johnson B,V, or R filters.

Table 1 - Dates and Filters for M81, M101, and M51

Date	M81	M101	M51
Nov 19 2006	B,R		
Nov 20	B,R		
Nov 24	R		
Nov 27	B,R		
Nov 28	B,R		
Dec 02	B,V,R		
Dec 21	B,V,R		
Dec 22	B,V,R		
Dec 25	B,V,R	B,V,R	
Dec 26	B,V,R	B,V,R	
Jan 02 2007	B,V		

Table 1 continued - Dates and Filters for M81, M101, and M51

Date	M81	M101	M51
Jan 03 2007	B,V,R	B,V	
Jan 04	B,V,R	B	
Jan 07	B,V,R	B,V	
Jan 10	B,V,R	B,V,R	
Jan 14	B,V,R		
Jan 15	B,V,R	B	
Jan 23	B,V,R	B,V,R	B,V,R
Feb 07		B,V,R	B,V,R
Feb 08		B,V,R	B,V,R
Feb 12		B,V,R	B,V
Feb 15	B,V,R	B,V	
Feb 16	B,V,R	B,V	
Feb 23	B,V,R	B,V,R	B,V
Feb 24	B,V,R	B,V,R	B,V
Feb 27	B,V,R	B,V,R	B,V,R
Mar 03		B,V,R	B,V,R
Mar 04		B,V,R	B,V,R
Mar 07		B,V,R	B,V,R
Mar 11		B,V,R	B,V,R
Mar 12		B,V,R	B,V,R
Mar 15	B,V,R	B,V,R	B,V,R
Mar 16	B,V,R	B,V,R	B,V,R
Mar 28		B,V,R	
Apr 01		B,V,R	B,V,R

Chapter 3

Data

3.1 Data Reduction

As previously stated this study was to compare the results of aperture photometry with PSF fitting using DAOphot. Using either method, though, we still must get photometry from standard stars and compare it against the nuclear light. I have included a brief synopsis of this process for the benefit of the reader. For a more thorough description of this process with some specific details about this particular CCD and its calibration frames, see the senior thesis of my research partner. [Johanson (2007)]

We used Image Reduction and Analysis Facility (IRAF) software to process all of our frames. This software was produced by the National Optical Astronomy Observatory, and is basically the program of choice at BYU for photometric analyses.

The first step in preparing the frames for data analyses is to take each frame through the calibration process to remove variations from the detector response. Every CCD chip introduces additional photon counts that do not actually originate from the stars being observed, so these extra counts must be removed to improve the mea-

surements of starlight. We accomplish this by taking three sets of calibration frames: Bias, Dark, and Flat.

A Bias frame is a frame taken by the CCD with a zero second duration. Basically, the CCD chip just unloads any counts that are already present on the chip due to the electrical current already in the chip and the time it takes the chip to unload the counts after the frame is taken. The number of counts is different for each pixel. We take several bias frames and average them pixel-for-pixel and combine them into one average bias frame. The counts on the bias frame are then subtracted pixel-for-pixel from each subsequent frame.

The Dark frame is a frame taken with the shutter closed for the same amount of time as the frames that you are intending to take of the actual objects. This frame should account for any extra counts introduced by the electrical current in the chip while the CCD is taking the picture. The number of counts should scale with time but will be different for each pixel again. The darks are combined and averaged again pixel-for-pixel and subtracted from each subsequent frame.

The last calibration frame is called a flat frame and is taken of a patch of sky with a uniform luminosity. This frame should be taken at dusk and should account for the difference in light response from pixel to pixel. Each pixel has a different light sensitivity. This calibration flattens the frames so that each pixel scales evenly. Flat frames must be taken in each filter, and each set is averaged together to make an averaged or master flat for each filter. After the bias and dark frames have been applied to an object frame, the flat frame is divided, rather than subtracted, into the object frame to even the pixel response levels.

3.1.1 Aperture Photometry

Aperture photometry is a classic method of measuring light and is simply the sum of all photons in an aperture centered on the object. Using the apphot software package of IRAF, we set an aperture size and center apertures over the standard stars and galactic nuclei of the reduced frames. Figures 3.1 through 3.3 show M81, M101, and M51 respectively with the nucleus labeled as 1 and comparison stars labeled with other numbers. Figure 3.3 also shows the companion nucleus of M51 labeled as 2.

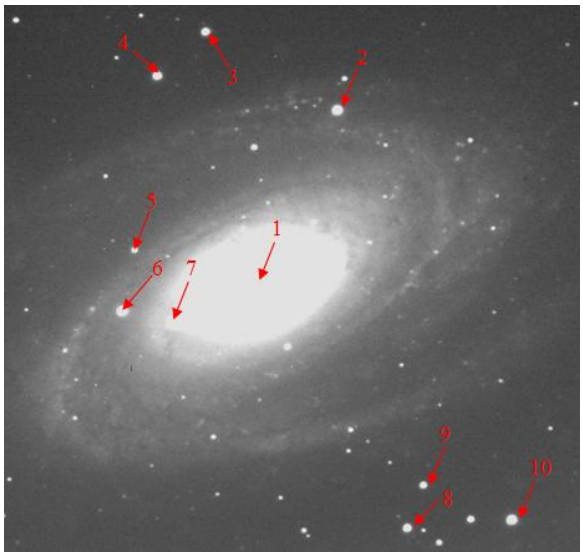

Figure 3.1 M81 and comparison stars

IRAF then sums the number of counts inside each aperture. The apertures must be recentered with each frame due to tracking errors from frame to frame. This makes the photometry portion of data reduction one of the more time consuming tasks. IRAF totaled the counts in each pixel and even scaled the counts for fractions of pixels contained within the aperture. IRAF also subtracted background counts from the aperture that came from sky brightness mainly. The number of counts was then converted to a flux by dividing by the exposure time and was then converted

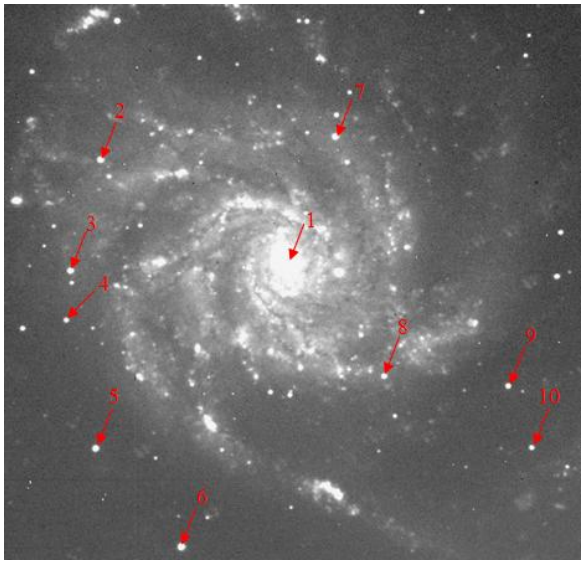

Figure 3.2 M101 and comparison stars

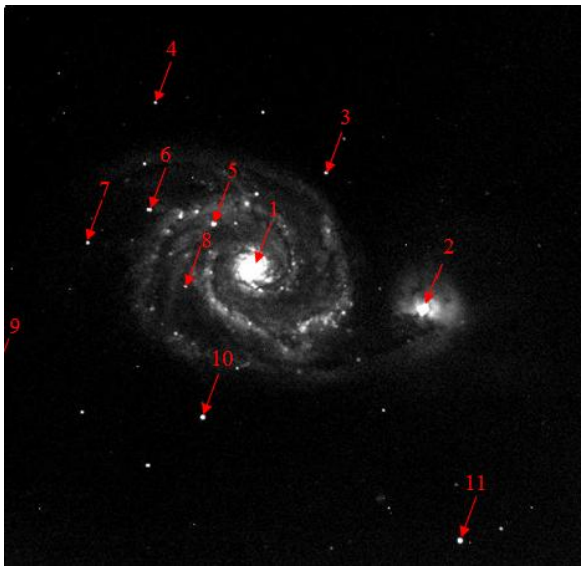

Figure 3.3 M51,companion galaxy and comparison stars

to a stellar magnitude using the equation M=-2.5*log(flux). We made photometric measurements on the galactic nuclei as well as the nine brightest stars in each frame. We used aperture sizes of 3 pixels, about one full-width half-maximum (FWHM) of the stellar light curves, and also 6 pixels, which was where the light curves blend in to the background.

3.1.2 DAO Photometry

We also used an additional package in IRAF called DAOphot to make measurements. DAOphot determines and mathematically fits the point spread function introduced on the stellar images using a numerical deconvolution. We selected several stars on each frame and images of the light profiles are shown in sequence. We then approved or declined each star based on whether or not it looked like a good candidate to determine the point spread function. A good candidate looks roughly Gaussian. We threw out candidates that did not have clearly defined PSFs or that looked saturated. We also did not include the galactic nuclei in this process because they are extended images with non-gaussian profiles. Figures 3.4 through 3.6 show examples of these three profiles respectively as they appear in the IRAF program using DAOphot.

Once we had selected at least six candidate stars, the software package determined a sort of average PSF and then deconvoluted each object before performing photometry on them. This process was the most time consuming portion of all the data reduction as we had to set several parameters for each different frame. Specifically, we had to find the gain and the read noise for each individual frame. We also had to determine the pixel radius for the average star in each individual frame as well as the pixel radius where the star's luminosity profile fades into the background noise. We made photometric measurements on the same objects for this process as we did for the regular aperture photometry.

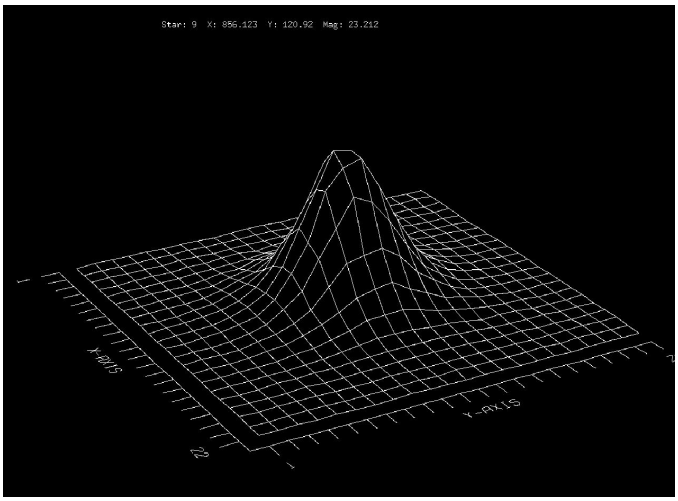

Figure 3.4 An example of the roughly-Gaussian profile of a star

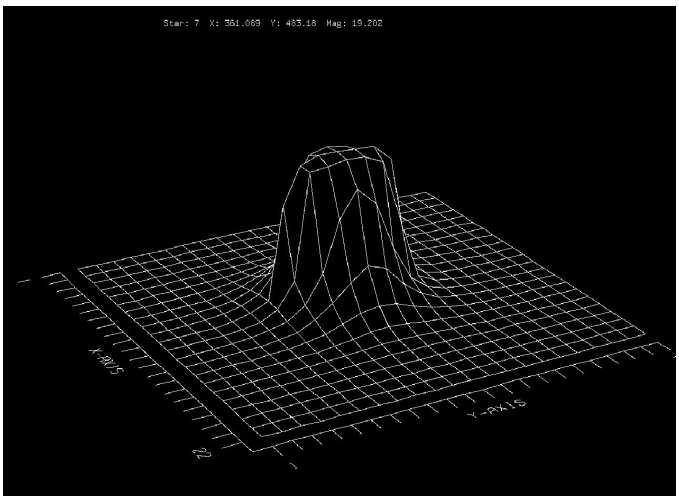

Figure 3.5 An example of the profile of a saturated star

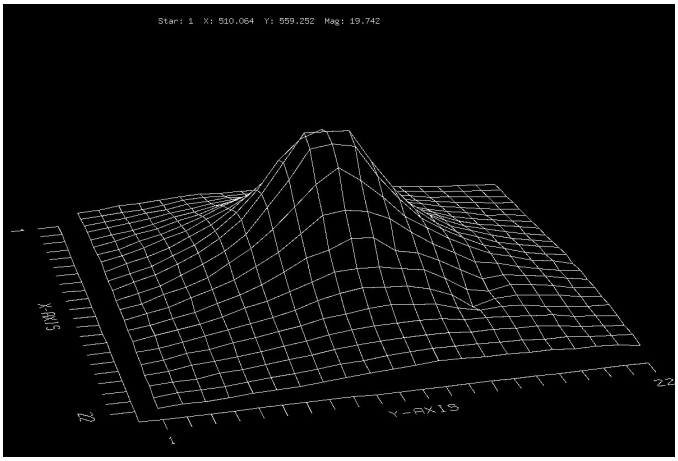

Figure 3.6 An example of the profile of a galaxian nucleus

Chapter 4

Analysis

Once we had obtained the magnitudes of each star on each night, we corrected for nightly variation due to seeing effects. Short term changes in humidity and atmospheric density change the apparent sizes and brightnesses of the stars from frame to frame and from night to night. This short term fluctuation accounts for most of the variation we observe on the simple plot of magnitude versus time. This is even more apparent when we plot all of the stars from all of the frames of a particular figure versus time. All of the objects have the same general trend of light versus time even though they may be parsecs away from each other.

To remove this common trend we used Microsoft Excel to calculate the observation error for each star over the entire period of observation. We used the equation

$$\sigma = \sqrt{\overline{x^2} - \overline{x}^2} \tag{4.1}$$

where

$$\sigma \tag{4.2}$$

is the average deviation from the mean and

$$\overline{x} \tag{4.3}$$

is the average magnitude of an object over our data set. We then found the star in our set with the least error per observation and used it as a standard. We subtracted the magnitudes of all the remaining stars from those of the standard star on a frame-by-frame basis to produce a set of differential magnitudes. The most stable stars should change in parallel with each other from frame to frame, so the difference between stable stars and the standard star should be constant from frame to frame. Using this method we could more easily see the activity of the galactic nuclei (See the appendix for the differential magnitude graphs). The stable stars should appear as straight lines of constant difference, while the nuclei should show some extra variation. We calculated the error again for the difference of each star and the standard star.

4.1 M81

Undoubtedly, the 3-pixel aperture allowed us to obtain much more accurate results than the 6-pixel aperture (Compare graphs A.1 and A.3 in Appendix A to B.1 and B.3 in Appendix B). Also, the B and V filters captured more variation in both apertures than the R filter did. For the V filter, the most stable star was star 9, with a maximum peak-to-peak variation of 0.041 magnitudes and a standard deviation of 0.0122. In comparison, the maximum peak-to-peak variation of the nucleus was 0.558 magnitudes with an standard deviation of 0.0809.

After using the DAOphot package to remove the point spread function from the image, we were able to achieve even better results. Interestingly, the PSF removal worked best with the R filter. The most stable star was star 8, which varied up to 0.092 magnitudes and had an average deviation of 0.0183. The nucleus varied up to 0.610 magnitudes and had an average deviation of 0.147. My research partner's results were worse when he used DAOphot on M81. As you can see, my results are to

the contrary, and DAOphot shows the variablilty of M81 much more than the 3-pixel apphot.

4.2 M101

For M101, the 3-pixel radius was also much better than the 6-pixel one. The B filter worked the best, with the most stable star being star 3. It varied up to 0.041 magnitudes with the average deviation being 0.00859. The nucleus varied up to 0.413 magnitudes with an average deviation of 0.0890. The V filter at 3 pixels showed the most stable star, star 3, with variability up to 0.037 magnitudes and stability of 0.00755. The nucleus showed variability of 0.289 magnitudes with average deviation of 0.0630.

We used the DAOphot package to again obtain better results. Unlike with M81, the B and V filters were the best with or without the PSF fitting. For the V filter, stars were stable down to 0.051 magnitudes with deviations of 0.0121. The nucleus varied with 1.025 magnitudes and deviated by 0.277.

4.3 M51

There were not as many frames taken of M51, so the results are not quite so stunning. However, the end results are the same. The 3-pixel aperture was much better than the 6-pixel aperture. Best results this time were with the R filter with stars stable down to 0.036 magnitudes with deviations of 0.00941. Nucleus 1, the nucleus of M51, varied by 0.171 magnitudes and had an average deviation of 0.0435. Nucleus 2, the companion nucleus, varied by 0.145 magnitudes and had an average deviation of 0.0336.

After removing the general PSF with DAOphot, the stars were stable down to 0.099 magnitudes with average deviations of 0.0292. Nucleus 1 varied by 0.511 magnitudes with average deviation of 0.146, and Nucleus 2 varied by 1.116 magnitudes with an average deviation of 0.240. As you can see, the results for M51 are not quite so dramatic, but they do show that DAOphot improves the results.

4.4 The Three Methods

The first observation we want to point out is that using a 6-pixel aperture to perform photometry on galaxian nuclei similar to those used in this data set is basically useless. The plots of M81 in Appendix A show the most success we achieved using the 6-pixel radius, which still wasn't very good. There are a couple of points on the right side of the plots that show a slight increase in luminosity for the galactic nucleus. In many cases, the reference stars appeared to be less stable than the galaxy. On average, the standard error for the galactic nuclei was only 1.57 times that for the standard stars in the B filter, 1.70 for the R filter, and 1.76 for the V filter. Apparently, a 6-pixel radius includes far too many bulge stars to show much change in luminosity.

The 3-pixel radius shows a little more fluctuation. We can see that the nuclei exhibit significant deviation from the relatively flat lines of the stars. On average, the error for the galactic nuclei was 3.49 times that of the comparison stars in the B filter, 4.31 in the R filter, and 3.30 in the V filter. So, we can see a larger distinction by using a 3-pixel radius.

The DAOphot exhibited far more fluctuation. On average, the standard error for all four galactic nuclei was 10.93 times that of the comparison stars in the B filter, 11.64 in the R filter, and 20.63 in the V filter. This method shows roughly an order of magnitude more detail in nuclear variability. However, if you compare the

trend of the nuclei in the DAOphot plots with that in the 6-pixel aperture plots (e.g. plots 16 and 25 in the appendix), they are quite different. The DAOphot method seems to introduce a lot more outliers that may or may not be actual luminosity measurements. It also drastically increases the peak-to-peak differences in some of the light curves, especially in the data series for M101. So, while it does seem to show more sensitivity to the light fluctuations, this method may or may not be illustrating the true luminosity curves for the nuclei. This error may be due to the nuclei not being point sources.

Chapter 5

Conclusion

We have gathered a good set of data for the luminosity variation of M51 and its companion, M81, and M101. We have also determined which stars may make good comparison stars.

We have shown a table of observation errors for the stars near each of these galaxies. We have also proven that, contrary to the results of my research partner, DAOphot does improve the apparent sensitivity of the results for all of these galaxies. However, we feel skeptical toward the results obtained using DAOphot. The DAOphot program seemed to amplify the luminosity fluctuations, alter the luminosity trends of the nuclei, and introduce far more outliers. We do not recommend this method for photometry of AGN.

The most important goal we have achieved, however, is to start the long process of observation for these three galaxies. We have laid the foundation for a 10-15 year study of the nuclear fluctuations of M81, M101, and M51. In time we hope to note some periodicity or other signature in these light curves that could be used to understand what is happening inside the nuclear bulge. We also expect to see some improvement on the observation and data analysis techniques for these types

of galaxies. These types of long term observations and improvements will give the astronomical community a better grasp on the role of black holes in galaxy evolution.

Bibliography

[Carrol et al. (1996)] Carroll, B., & Ostlie, D., 1996, *Introduction to Modern Astrophysics*, Addison-Wesley

[Freedman et al. (2005)] Freedman, R.A., & Kaufmann III, W.J., 2005, *Universe, 7ed.*, W. H. Freeman and Company

[Johanson (2007)] Johanson, A. 2007, Thesis(Undergrad), Brigham Young University

[Massey et al. (1992)] Massey, P., & Jacoby, G.H., 1992 ASP, 23, 245

[McNeil (2004)] McNeil, S., 2004, Thesis(PHD), Brigham Young University

[Schwartz (2007)] Schwartz, M. 2007, *www.tenagraobservatories.com*

[Sterken (1995)] Sterken, C. 1995, IAUS, 167, 134

[Van der Marel (1999)] Van der Marel, R.P., 1999, IAUS, 186, 333

Appendix A

Light Curves For 6-Pixel Aperture

Here are the differential magnitude plots of the galactic nuclei as well as the three most stable stars in the field for each frame. The differential magnitudes were obtained by aperture photometry using a 6-pixel aperture.

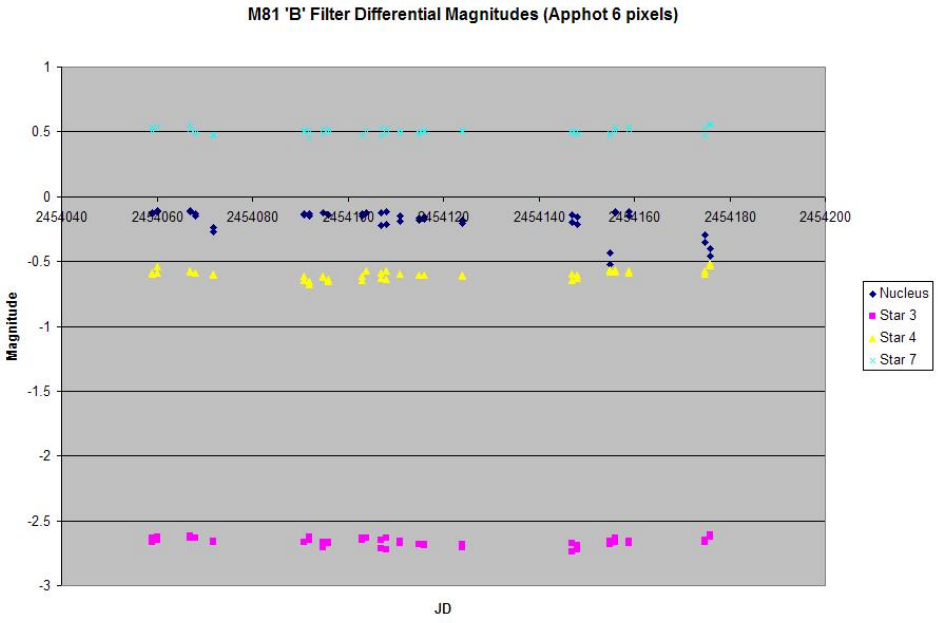

Figure A.1

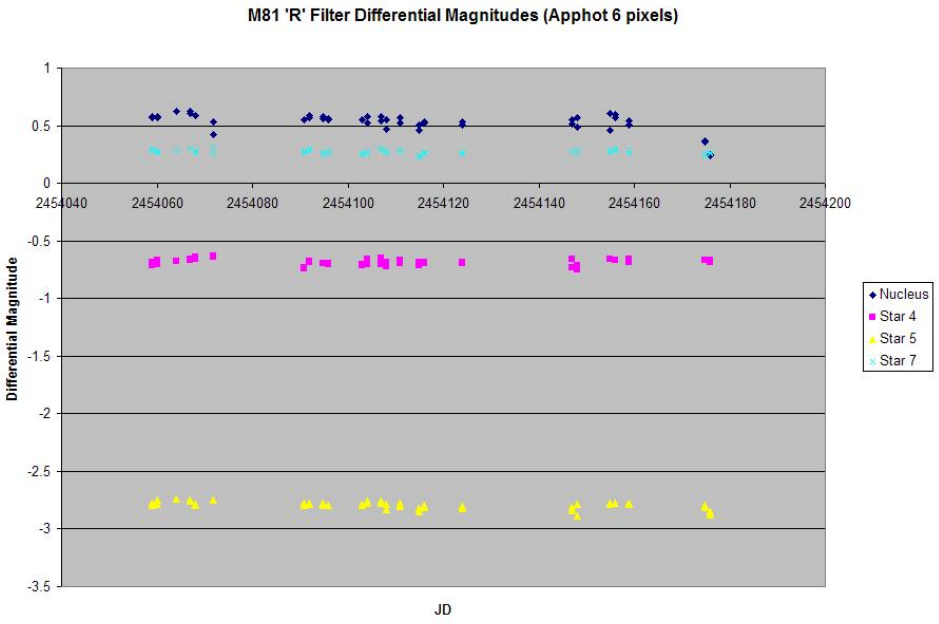

Figure A.2

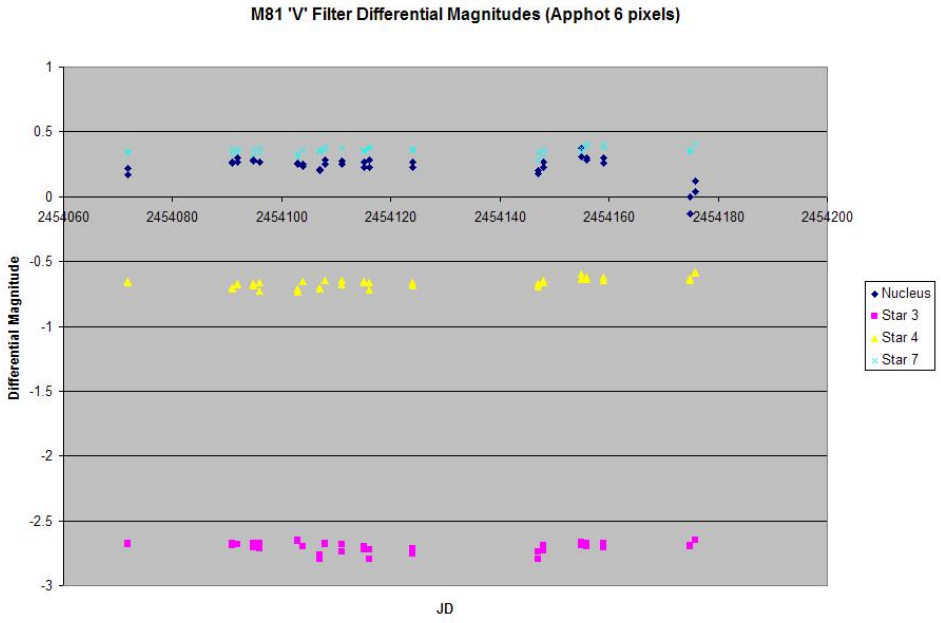

Figure A.3

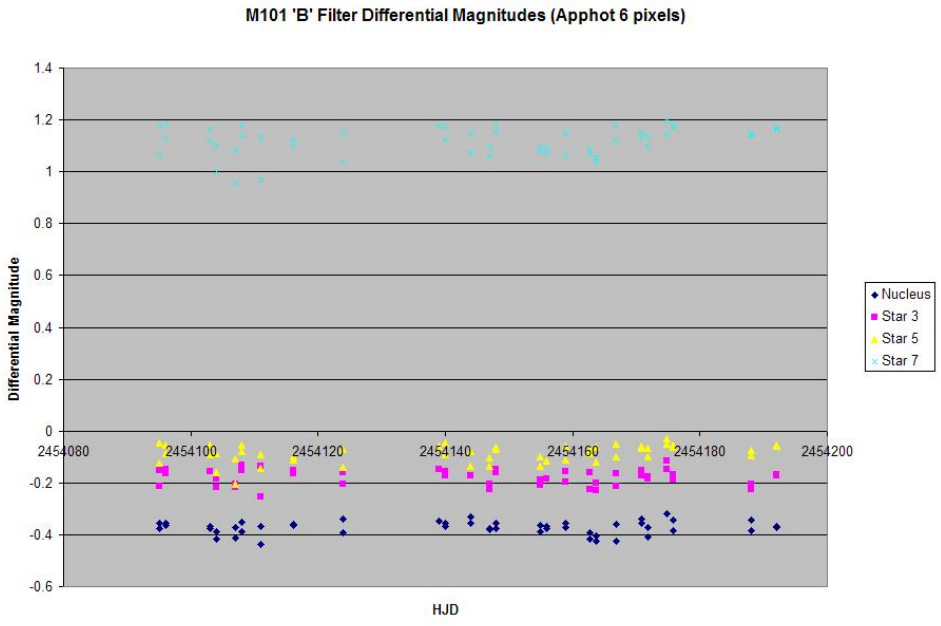

Figure A.4

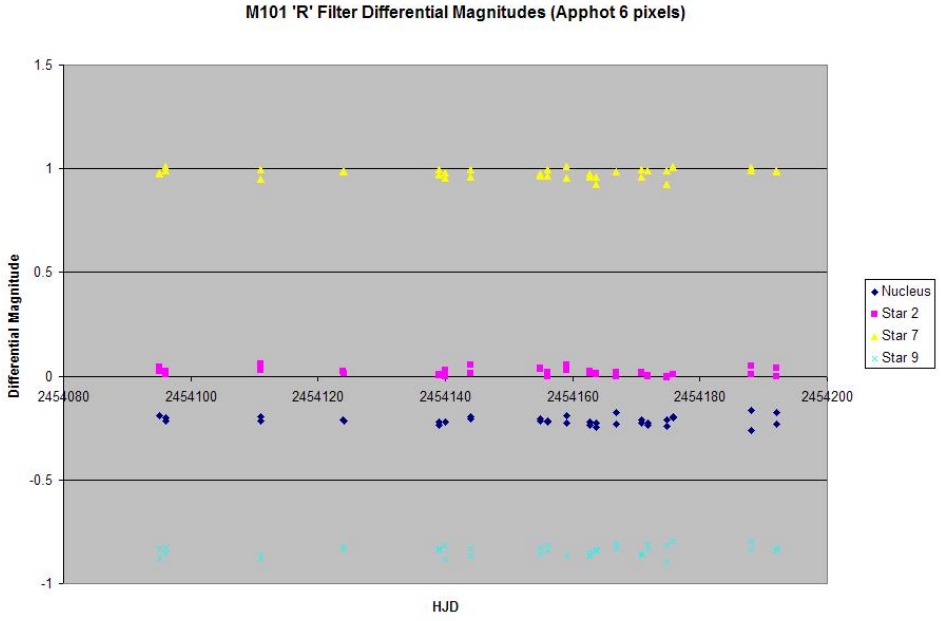

Figure A.5

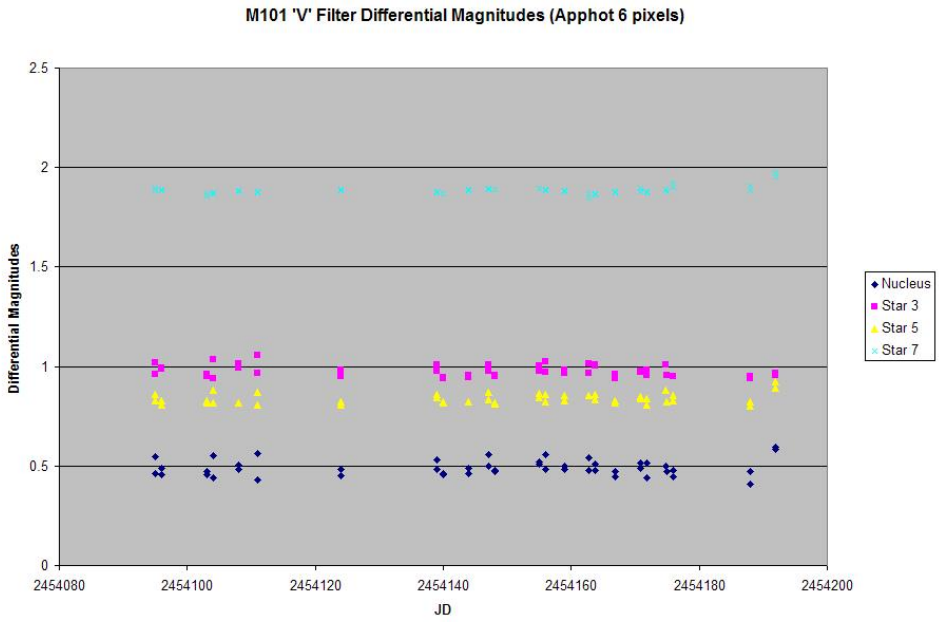

Figure A.6

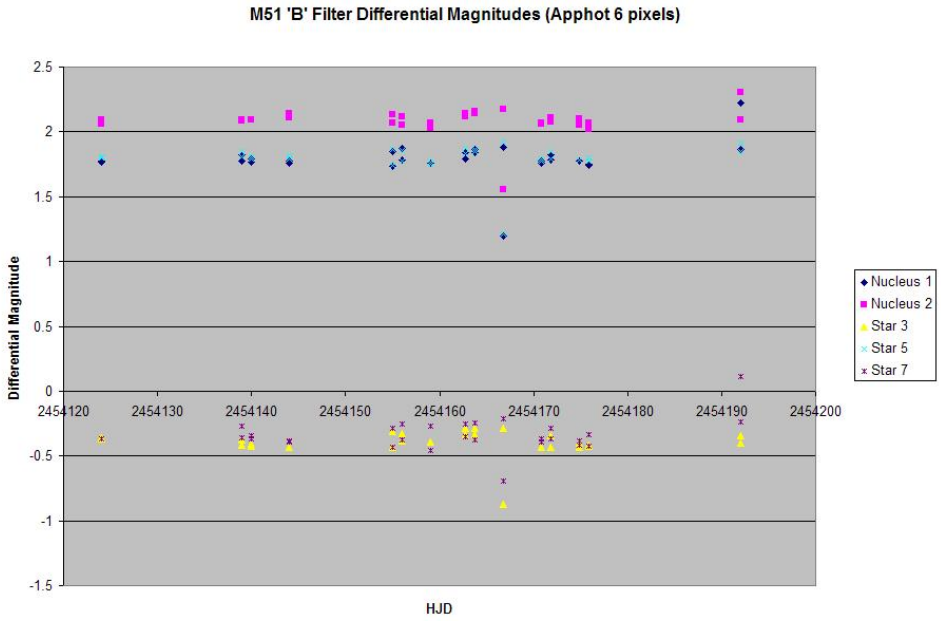

Figure A.7

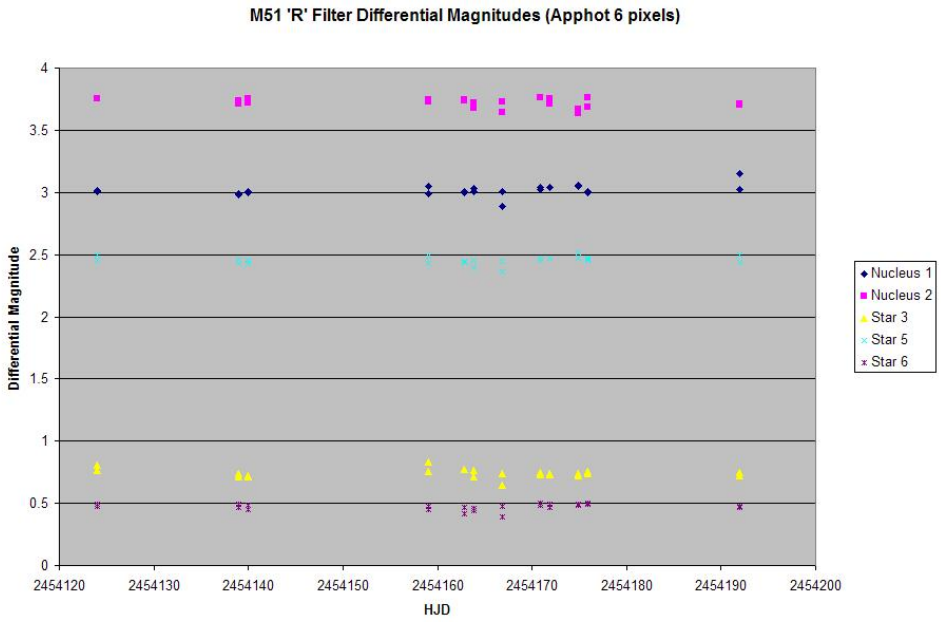

Figure A.8

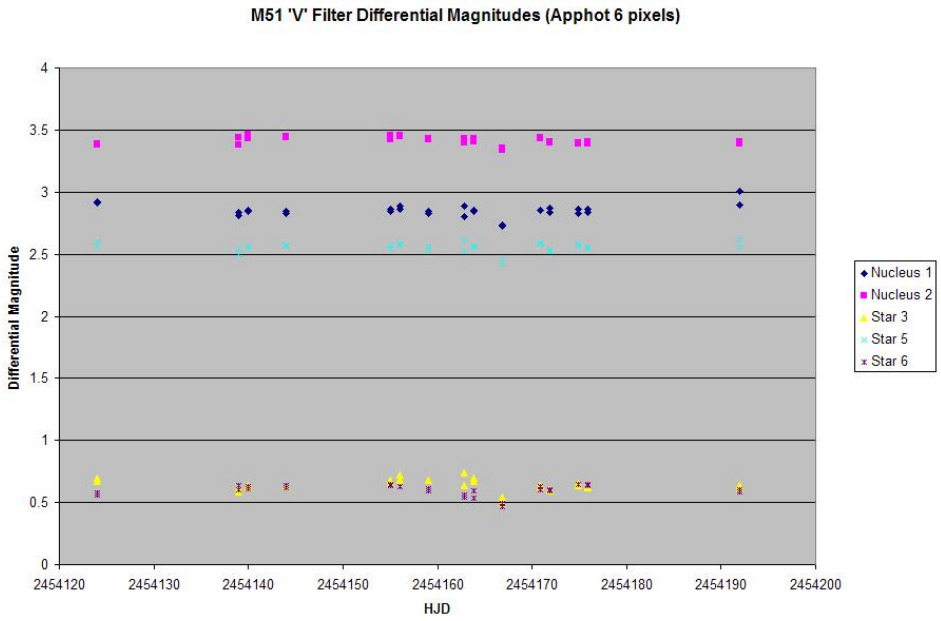
M51 'V' Filter Differential Magnitudes (Apphot 6 pixels)
Differential Magnitude
HJD
4
3.5
3
2.5
2
1.5
1
0.5
0
2454120
2454130
2454140
2454150
2454160
2454170
2454180
2454190
2454200
Nucleus 1
Nucleus 2
Star 3
Star 5
Star 6

Figure A.9

Appendix B

Light Curves For 3-Pixel Aperture

Here are differential magnitude plots for aperture photometry with a 3-pixel radius.

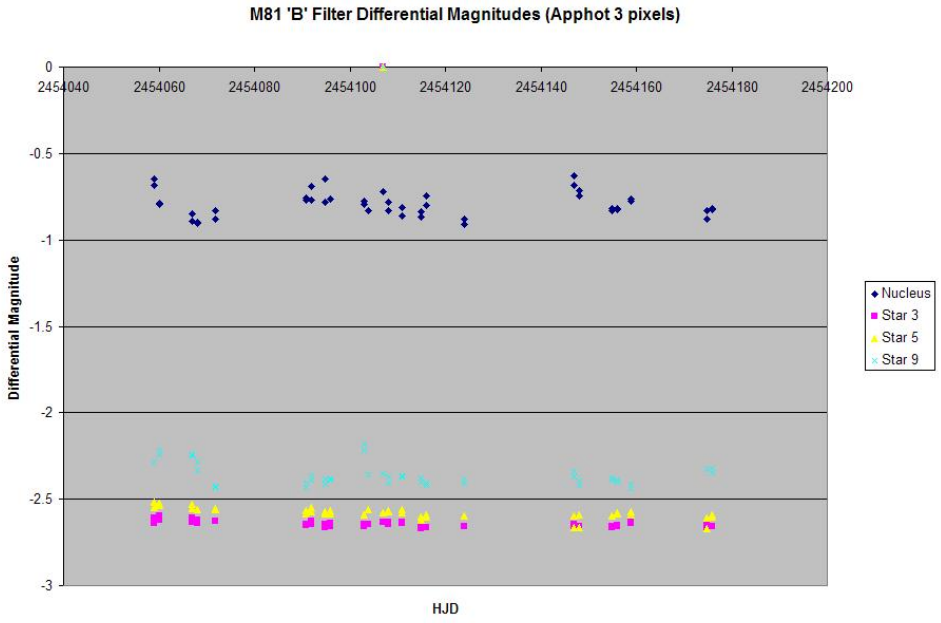

Figure B.1

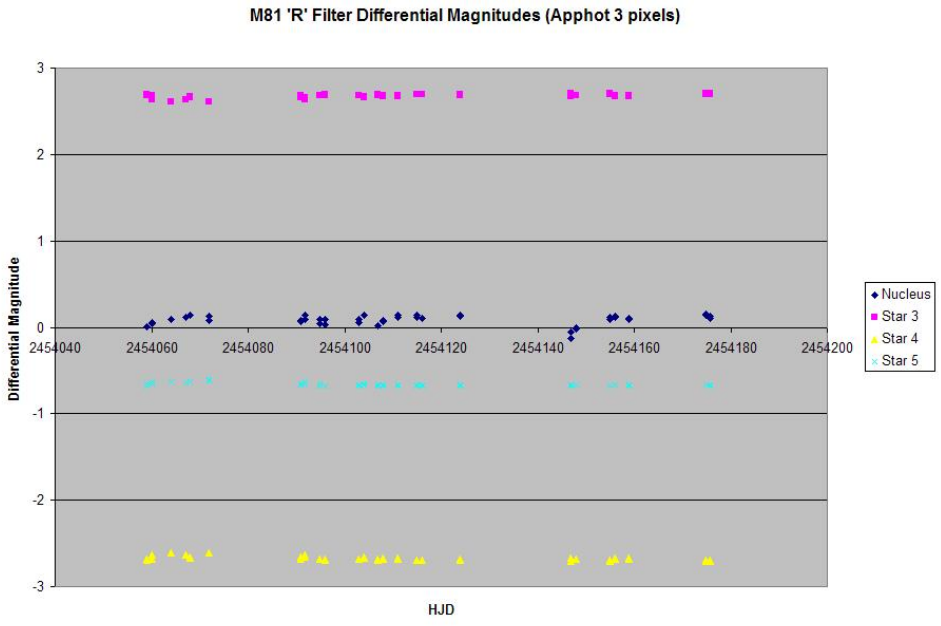

Figure B.2

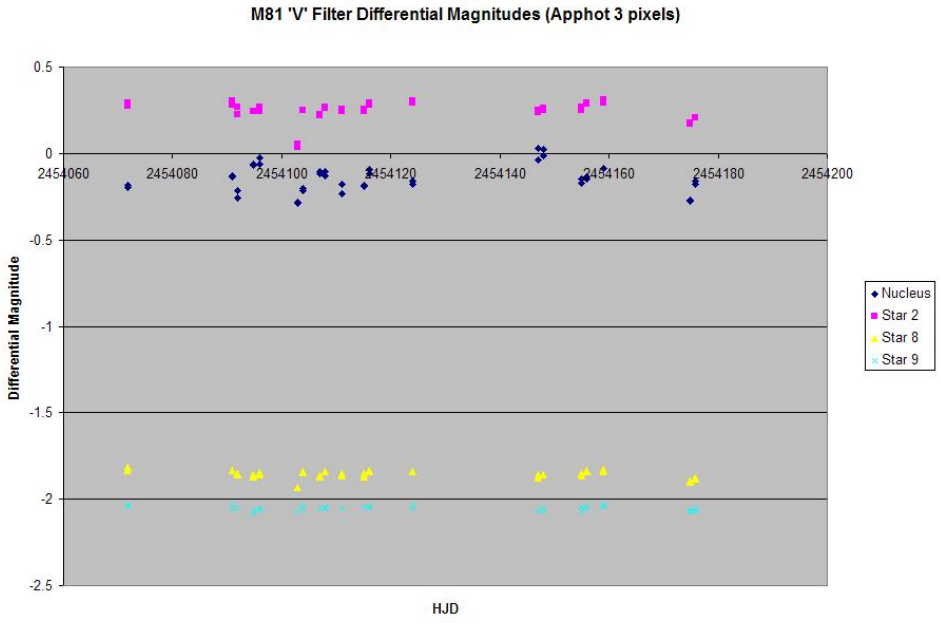

Figure B.3

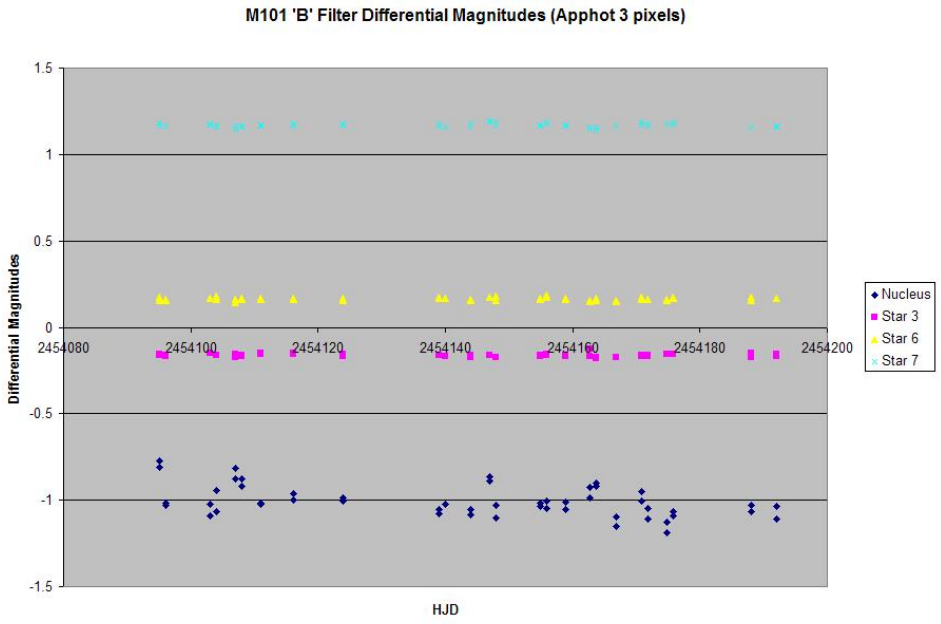

Figure B.4

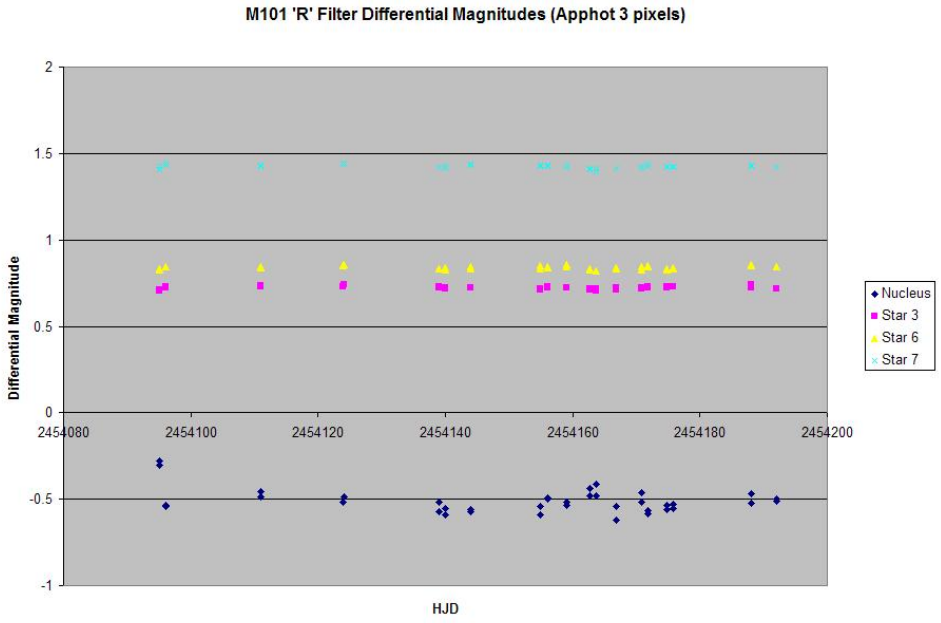

Figure B.5

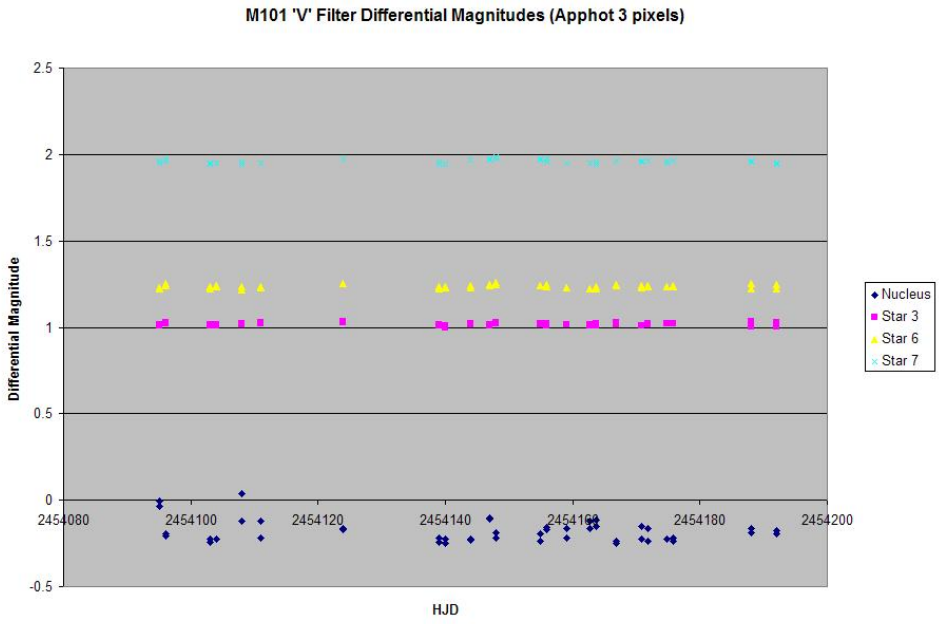

Figure B.6

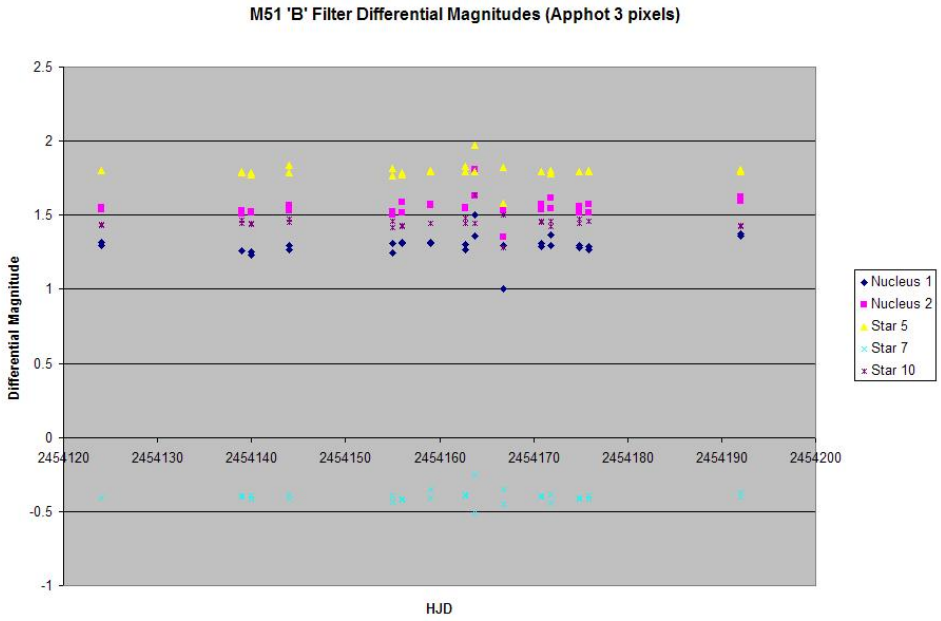

Figure B.7

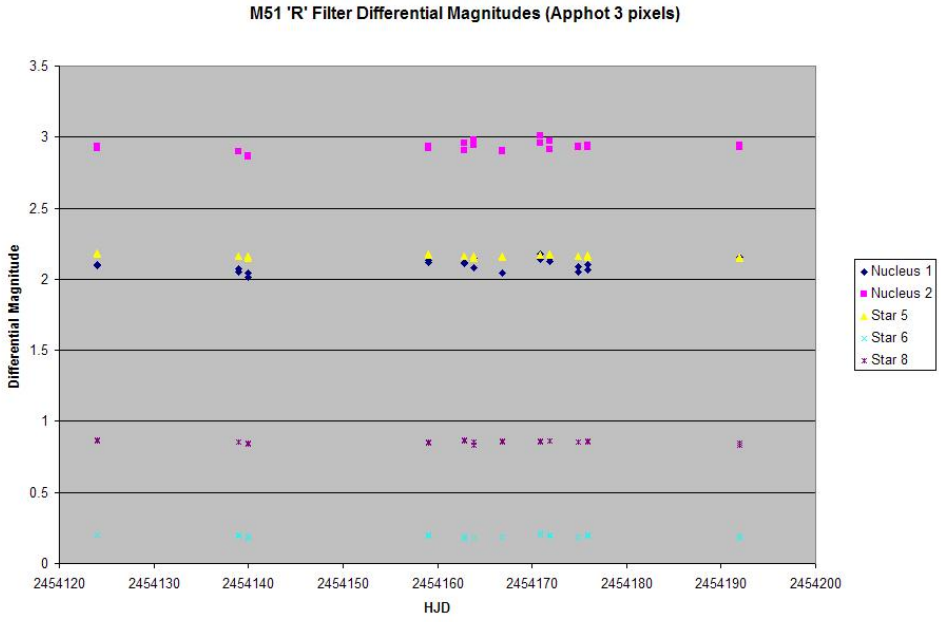

Figure B.8

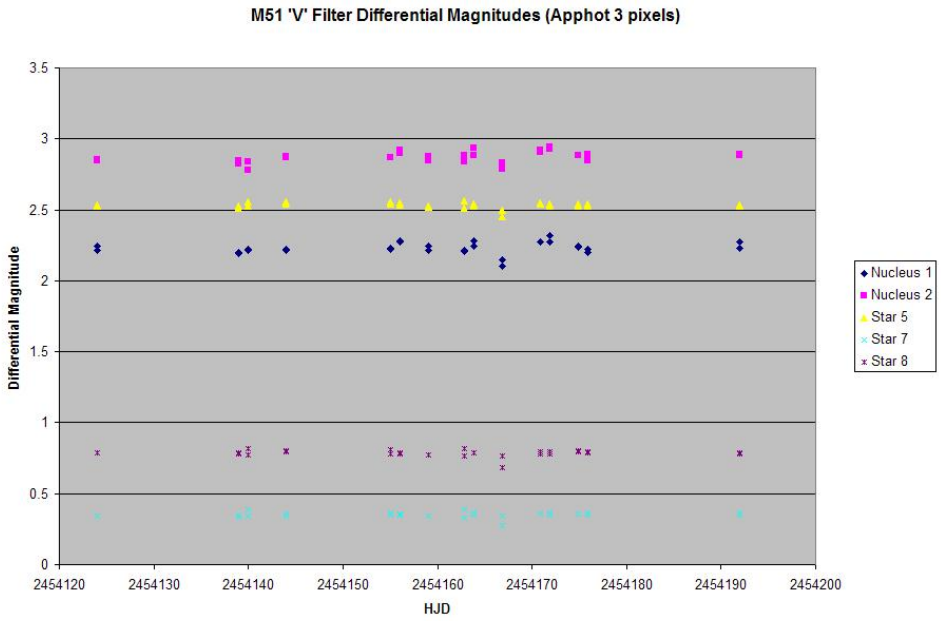
M51 'V' Filter Differential Magnitudes (Apphot 3 pixels)
Differential Magnitude
HJD
3.5
3
2.5
2
1.5
1
0.5
0
2454120
2454130
2454140
2454150
2454160
2454170
2454180
2454190
2454200
Nucleus 1
Nucleus 2
Star 5
Star 7
Star 8

Figure B.9

Appendix C

Light Curves For DAOphot

Here are the differential magnitude plots obtained using DAOphot, the PSF fitting method.

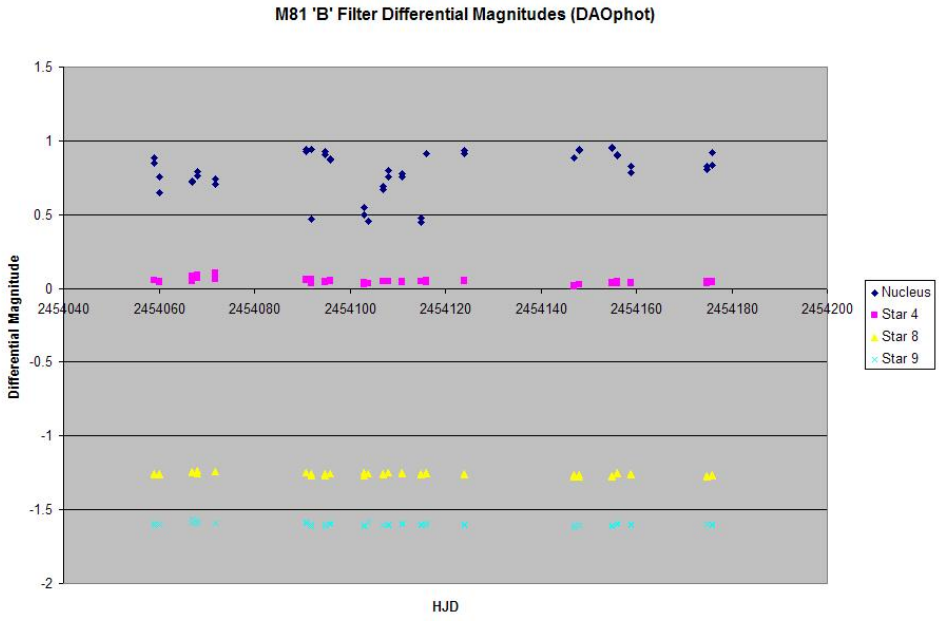

Figure C.1

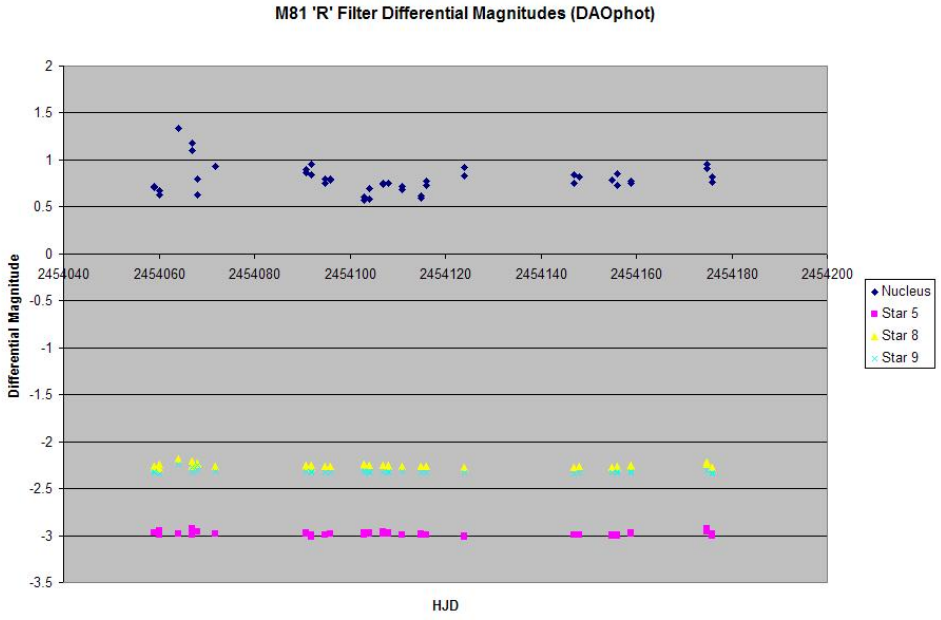

Figure C.2

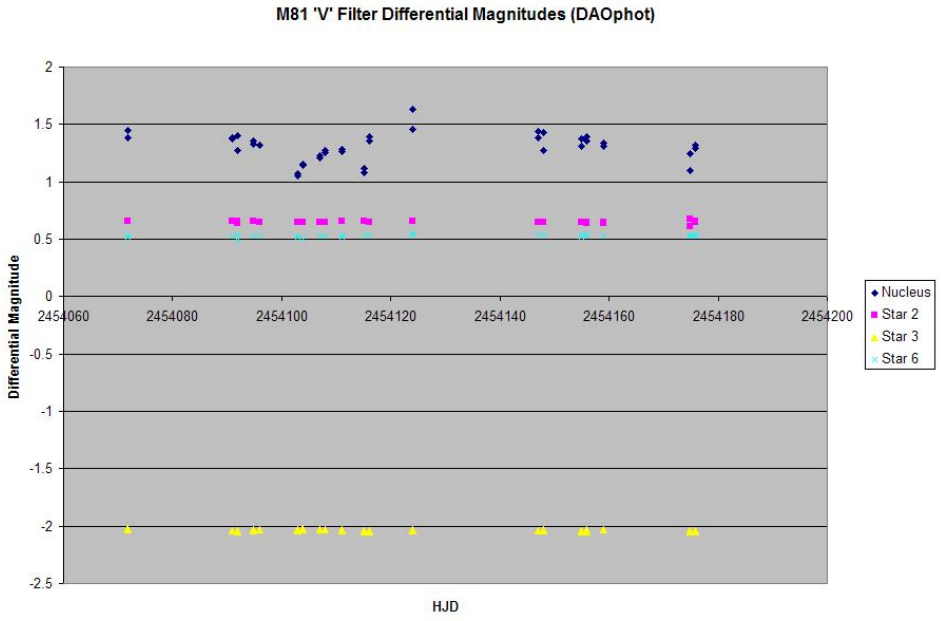

Figure C.3

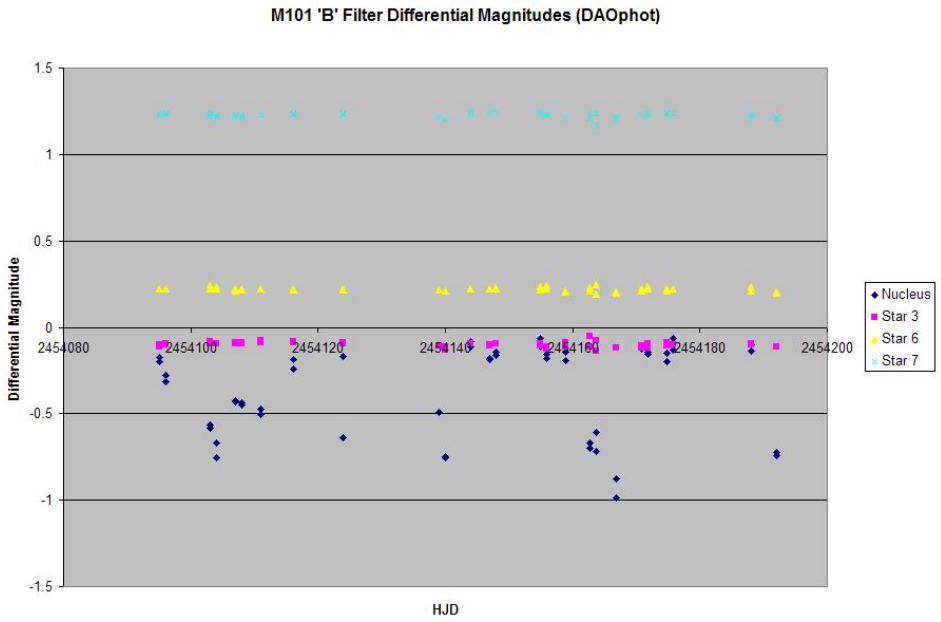

Figure C.4

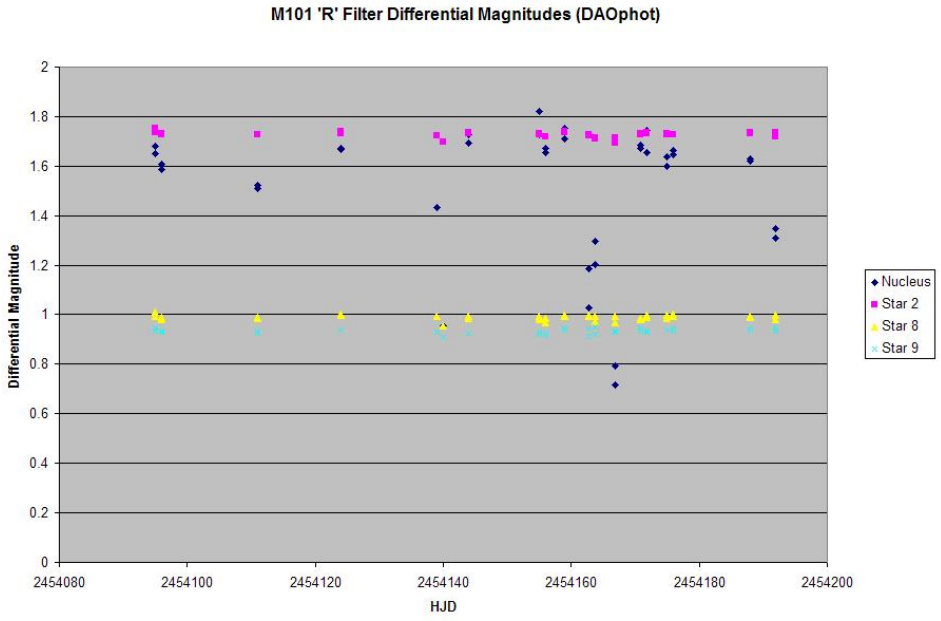

Figure C.5

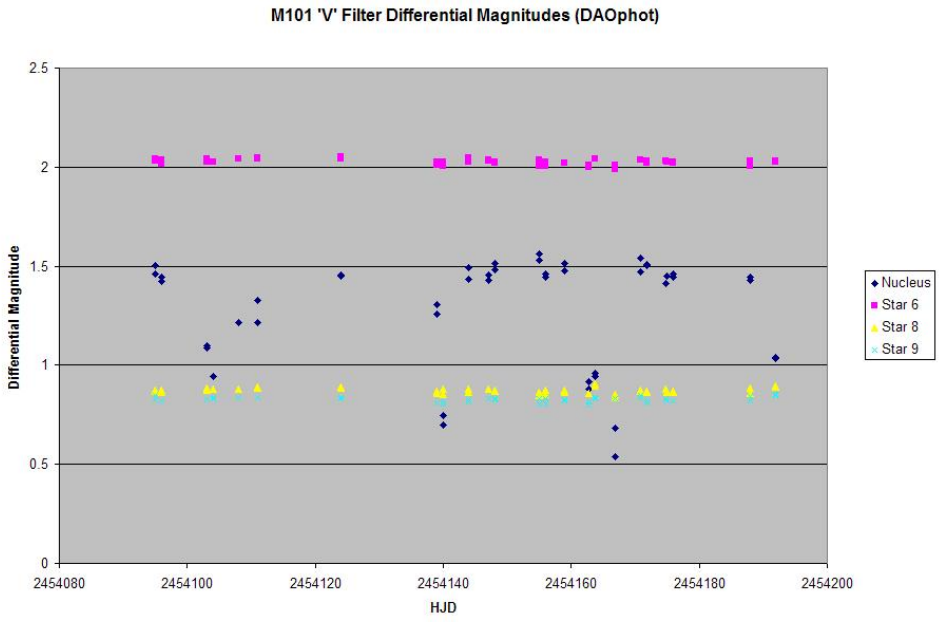

Figure C.6

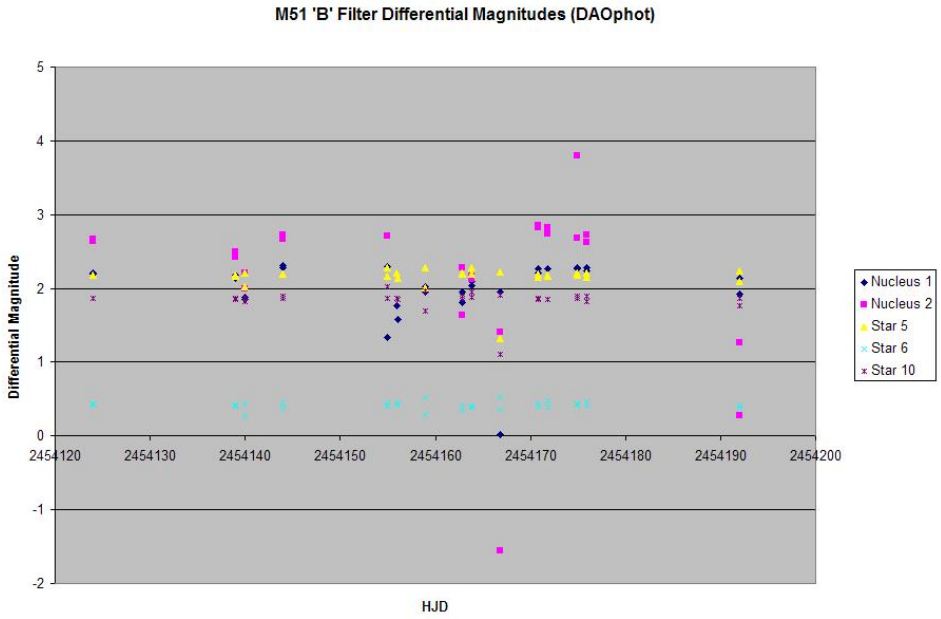

Figure C.7

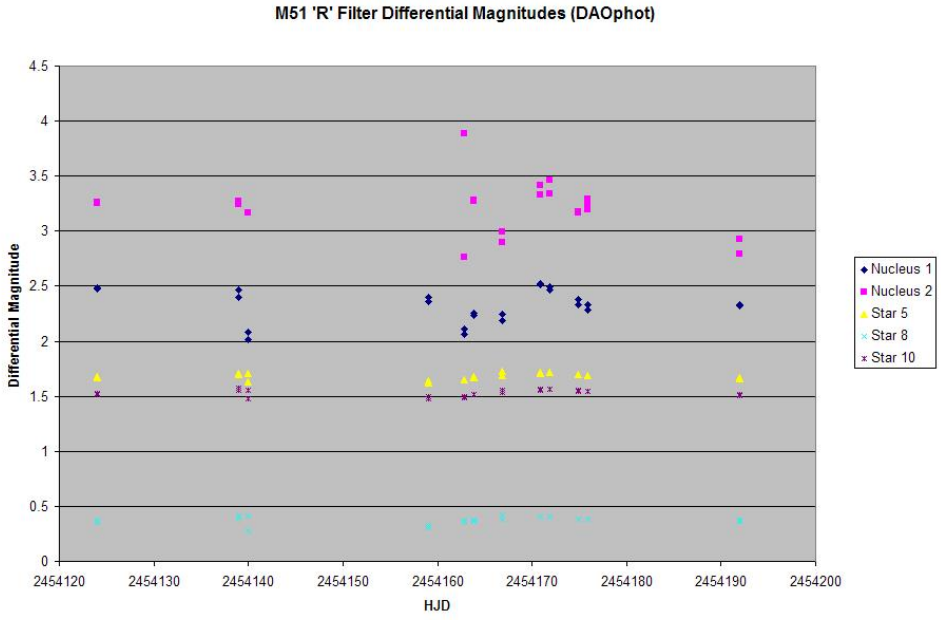

Figure C.8

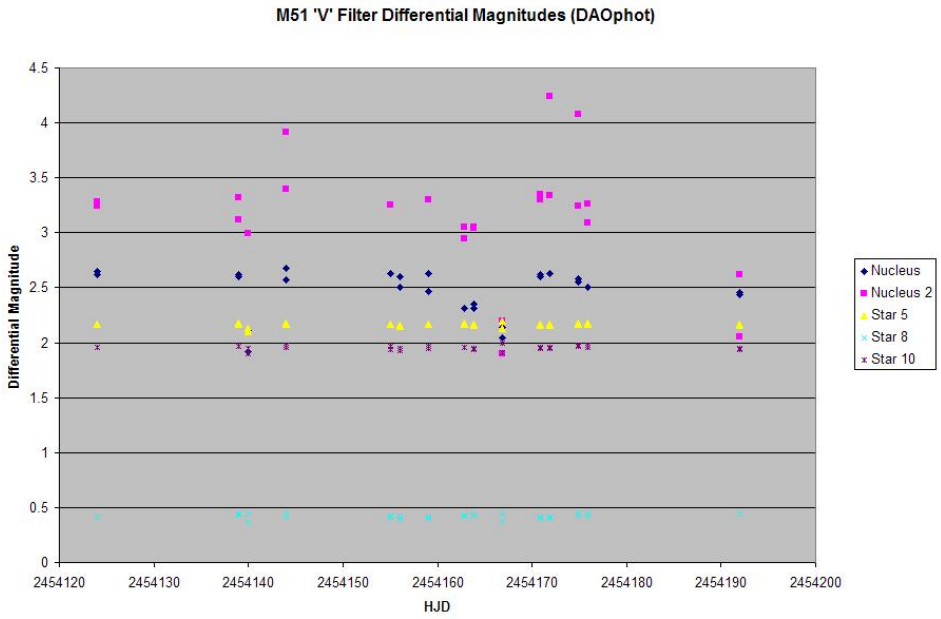
M51 'V' Filter Differential Magnitudes (DAOphot)
Differential Magnitude
HJD
4.5
4
3.5
3
2.5
2
1.5
1
0.5
0
2454120
2454130
2454140
2454150
2454160
2454170
2454180
2454190
2454200
Nucleus
Nucleus 2
Star 5
Star 8
Star 10

Figure C.9

Appendix D

Tables of Error Values

D.1 M81

This first table shows the errors calculated for the nucleus of M81. It also shows the average error values for the three comparison stars shown in each corresponding graph in the previous appendices.

	Nucleus	Comparison Stars
6-Pixel		
B Filter	0.09857	0.028962
V Filter	0.089506	0.024944
R Filter	0.0820365	0.025106
3-Pixel		
B Filter	0.0702604	0.037782
V Filter	0.0808699	0.031259
R Filter	0.0581476	0.022867
DAOphot		
B Filter	0.147157	0.01221
V Filter	0.1226445	0.00888
R Filter	0.1471072	0.01869

D.2 M101

This next table shows the errors calculated for the nucleus of M101 and the average error values for the three comparison stars shown in each corresponding graph in the previous appendices.

	Nucleus	Comparison Stars
6-Pixel		
B Filter	0.026063	0.040172
V Filter	0.040479	0.024992
R Filter	0.020604	0.021315
3-Pixel		
B Filter	0.088959	0.009755
V Filter	0.062981	0.009324
R Filter	0.06887	0.009841
DAOphot		
B Filter	0.26097	0.013162
V Filter	0.276552	0.009205
R Filter	0.278506	0.010677

D.3 M101

This last table shows the errors calculated for the nucleus of M51 as well as the companion nucleus (nucleus 2). The average error values for the three comparison stars in each corresponding graph are included as well.

	Nucleus	Companion Nucleus	Comparison Stars
6-Pixel			
B Filter	0.142475	0.112369	0.115252
V Filter	0.050674	0.031293	0.044979
R Filter	0.042816	0.036714	0.030977
3-Pixel			
B Filter	0.075835	0.068847	0.048318
V Filter	0.042452	0.038812	0.02096
R Filter	0.043502	0.033583	0.009991
DAOphot			
B Filter	0.441973	1.033782	0.124575
V Filter	0.200067	0.537851	0.01908
R Filter	0.14638	0.240268	0.030697